ResearchGate

See discussions, stats, and author profiles for this publication at: https://www.researchgate.net/publication/260295295

Fluid-Induced Propulsion of Rigid Particles in Wormlike Micellar Solutions

ARTICLE *in* PHYSICS OF FLUIDS · FEBRUARY 2014

Impact Factor: 2.03 · DOI: 10.1063/1.4896598 · Source: arXiv

CITATIONS
2

READS
32

4 AUTHORS, INCLUDING:

David A Gagnon
University of Pennsylvania
8 PUBLICATIONS **85** CITATIONS
SEE PROFILE

Nathan C. Keim
California Polytechnic State University, San L…
27 PUBLICATIONS **193** CITATIONS
SEE PROFILE

Paulo E. Arratia
University of Pennsylvania
107 PUBLICATIONS **1,315** CITATIONS
SEE PROFILE

Available from: Paulo E. Arratia
Retrieved on: 26 January 2016

arXiv:1402.5022v1 [physics.flu-dyn] 20 Feb 2014

Fluid-Induced Propulsion of Rigid Particles in Wormlike Micellar Solutions

David A. Gagnon,[1] Nathan C. Keim,[1] Xiaoning Shen,[1] and Paulo E. Arratia[1, a)]

Department of Mechanical Engineering and Applied Mechanics,
University of Pennsylvania, Philadelphia, PA 19104

(Dated: 21 February 2014)

In the absence of inertia, a reciprocal swimmer achieves no net motion in a viscous Newtonian fluid. Here, we investigate the ability of a reciprocally actuated particle to translate through a complex, "structured" fluid using tracking methods and birefringence imaging. A geometrically polar particle, a rod with a bead on one end, is reciprocally rotated using magnetic fields. The particle is immersed in a wormlike micellar solution that is known to be susceptible to shear banding and the formation of local anisotropic structures. Results show that the nonlinearities present in this structured fluid break time-reversal symmetry under certain conditions, and enable propulsion of an artificial "swimmer." We find three regimes dependent on the Deborah number (De): net motion towards the bead at low De, net motion towards the rod at intermediate De, and no propulsion at high De. At low De, we believe propulsion is caused by an imbalance in the first normal stress differences between the two ends of the particle (bead and rod). However, at $De \sim 1$, we observe network anisotropy near the rod using birefringence imaging, indicating alignment of the micellar structure, which is "locked in" due to the shorter timescale of the particle relative to the fluid. The development of these structures reverses the direction and magnitude of the imbalance in first normal stress differences, and suggests the particle is actively remodeling the microstructure, thus providing the nonlinearity required for propulsion.

[a)]Electronic mail: parratia@seas.upenn.edu

I. INTRODUCTION

Many microorganisms, including various single-cell eukaryotic protozoa (e.g. sperm cells[1–3]), prokaryotes (e.g. bacteria[4]), and multi-cellular organisms (e.g. nematodes[4,5]) live in low Reynolds number environments. In such environments, linear viscous stresses that scale as $\sim \mu U/L$ are much larger than nonlinear stresses from fluid inertia that scale as $\sim \rho U^2$, where U is a characteristic velocity, L is a length-scale, and ρ and μ are the fluid density and viscosity, respectively. For microorganisms swimming in simple liquids, the ratio of inertial to viscous stresses, calculated using the Reynolds number $Re = \rho UL/\mu$, is often very small ($Re \ll 0.1$) due to their small length scale ($L < 10^{-4}$ m). At low Re, fluid flows have time-reversal symmetry and net locomotion can only be generated from non-reciprocal kinematics that break this symmetry;[1,6,7] this restriction is also known as the "scallop theorem."[8] Microorganisms have developed different strategies to move at low Re, as seen in the rotating flagella of *E. coli*,[9] the sinusoidal undulations of *C. elegans*,[10] and the cilial beating of *Paramecium*.[6] While much work has revealed the details of propulsion at low Re in Newtonian fluids,[6] many natural environments encountered by microorganisms, from bacterial films to blood, contain polymers and/or particles and are not Newtonian. Cervical fluid and gastric mucus, for example, have been shown to possess non-Newtonian behavior including viscoelasticity and rate dependent viscosity, and are successfully navigated by microscopic swimmers.[11–14] Recently, theoretical and numerical studies[15–19] as well as experiments[20–22] have shown that viscoelasticity can significantly affect the ability of an organism to propel itself by modifying the swimmer's kinematics, particularly its propulsion speed. Whether fluid elasticity enhances or hinders self-propulsion seems to depend on the type of kinematics employed by the organism (e.g. undulating waves or rotating helices) and its interactions with the fluid microstructure (e.g. polymer molecules and networks).

As briefly mentioned above, many investigations have shown that the nonlinear rheological behavior (e.g. viscoelasticity) characteristic of many complex fluids can modify the swimming behavior of microorganisms. Another possibility is that complex fluids possessing nonlinear rheology and/or structure (e.g. polymer networks) can *enable* rather than just modify propulsion. Such "fluid-induced" propulsion at low Re has been theoretically predicted for idealized viscoelastic fluids.[23,24] By solving the Stokes' equation along with the Oldroyd-B constitutive model for viscoelastic fluids, it was shown that propulsion at low Re

is possible for flapping surfaces,[23,24] "squirming" of a sphere with surface oscillations,[25] and a cylinder with a reciprocal stroke but direction-dependent rates.[26] A recent experimental investigation has indeed shown that the extra elastic stresses present in dilute polymeric (viscoelastic) solutions can break the constraint of kinematic reversibility (i.e. scallop theorem) at low Re and lead to propulsion even for a reciprocally actuated "swimmer."[27] This fluid-induced propulsion is not possible in simple, Newtonian fluids under the same conditions.

However, many fluids of practical interest found in nature and the human body are not dilute and often possess structure that arises from interactions or even cross-linking among polymer chains, for example. Many organisms are known to move, feed, and reproduce in highly structured fluids such wet soil,[28,29] human mucus,[30] and tissues.[31] The interplay between the fluid's internal structure (e.g. polymer networks) and self-propulsion is critical to many biological processes such as reproduction,[30] bacterial infection,[32] and biodegradation in soil.[33] Structured fluids possessing networks such as surfactant or wormlike micellar (WLM) solutions can exhibit many fascinating phenomena under applied stress including shear banding[34–36] and even fracture.[37–39] Despite recent advances (briefly discussed below),[18,28,31,40–42] the effects of the fluid networks and microstructure on swimming are still poorly understood.

The effects of fluid structure on swimming have been studied in theory[40,41] and in experiments[28,29,31,42,43] A theoretical analysis using the Brinkman model to approximate heterogeneous, gel-like environments showed that the fluid microstructure can lead to an enhancement in propulsion speed.[40] Note that the Brinkman model treats the heterogeneous media as static inclusions in a viscous fluid. Using a two-fluid model, which allows for both dynamic and stationary inclusions, Fu *et al.*[41] showed that the fluid network can enhance the propulsion of a infinite sheet when the microstructure is stiff and compressible. Experiments have also shown the fluid microstructure can significantly affect the motility behavior of living organisms. For example, *Escherichia coli* can exhibit enhanced propulsion speeds in non-dilute polymeric solutions,[43] *Caenorhabditis elegans* can swim faster in polydisperse (size) wet granular networks,[28,29] and that spirochetes in gelatin can exhibit four motility states that are highly dependent on gelatin concentration.[31] More recently, an experimental investigation showed that the swimming speed of *C. elegans* is enhanced in a concentrated polymer solution that supports the local alignment of polymer molecules.[42]

It was proposed that the swimmer's stroke aligns the polymer molecules, creating a local anisotropy; crowding of polymers at these concentrations creates a history dependence favorable to undulatory swimming. Effectively, the swimmer actively modifies the local properties of the fluid with its motion.[42]

In this manuscript, we investigate the ability of a reciprocally actuated particle to translate through a "structured" fluid. A geometrically polar particle, a rod with a bead on one end, is reciprocally actuated in a wormlike micellar (WLM) solution. These solutions are highly susceptible to fluid instabilities, shear banding, and the formation of local anisotropic structures.[36] At low strains and strain rates, we expect WLM solutions to behave like a nearly Maxwellian fluid.[44] Constitutive models, such as the Rolie-Poly model, combine the traditionally defined reptation time for the micellar network with micellar stretching and convective constraint release (CCR) to predict stability.[45–48] Ultimately, as the strain and strain rate are increased, we anticipate increasing nonlinearity in the mechanical properties of the fluid, and thus significant deviations from well-behaved models, which might explain any observed propulsion.

Our experimental results show that a reciprocally actuated rigid particle is indeed able to achieve net motion in a WLM solution (see Fig. 3), which indicates that kinematically reversibility has been broken. Furthermore, we find that the particle propulsion speed in the WLM solution is much faster, by almost an order of magnitude, than for dilute polymeric solution under similar conditions. This highlights the importance of the fluid microstructure in the present investigation. The behavior of the particle in the WLM solution is highly dependent on the period of oscillation and strain rate relative to the characteristic timescale of the fluid, described by the Deborah number $De = \lambda\omega$ and the Weissenberg number $Wi = \lambda|\dot{\gamma}|$, respectively, where ω is the angular frequency of the particle, $\dot{\gamma}$ is the strain rate, and λ is the relaxation time of the fluid. When the actuation period is much slower than the time required for the micellar network to heal and the fluid is stable ($De < 1.0$, $\overline{Wi} < 10.0$), we observe translation towards the end of the polar particle with the bead. When the period is approximately equal to the characteristic timescale of the fluid and the average strain rate becomes large ($De \sim 1$, $\overline{Wi} \gtrsim 10$), we observe the development of structure within the fluid near the rod-end of the polar particle, and the propulsion reverses direction. At periods much shorter than the relaxation time ($De > 10$), we observe no propulsion (cf. Fig. 4).

II. EXPERIMENTAL METHODS

In order to investigate fluid-induced propulsion, we consider two particle configurations: (i) asymmetric and (ii) symmetric, as shown in Fig. 1(a). The asymmetric particle is fabricated from carbon steel wire of length $2R_{\text{dimer}} \approx 3$ mm and diameter 230 μm with an epoxy bead of diameter $2R_{\text{bead}} \approx 1000$ μm placed at one end. These ends will be referred to as the "rod" and "bead" respectively throughout the manuscript. The symmetric particle has two epoxy beads with diameters $2R_{\text{bead}} \approx 1000$ μm, one on each end.

The particle is reciprocally actuated by four surrounding electromagnets, as shown in Fig. 1(b). Two diametrically opposed electromagnets produce a constant field $\vec{B}_{\text{align}}$ while an orthogonal pair of magnets generate an AC field $\vec{B}_{\text{drive}}$. The AC field is computer controlled and driven in the shape of a square wave with a ramp time $t_r = 0.05$ s, thus exerting a periodic torque τ_{mag} on the particle (Fig. 1(c)). Both the magnitude of $\vec{B}_{\text{align}}$ and amplitude of $\vec{B}_{\text{drive}}$ are on the order of 10^3 G.[27] The aligning magnitude and driving amplitude were kept constant and equal.

The magnetic fields actuating the particle are slightly inhomogeneous. While careful attention is paid to placing the particle in the center of the magnets, small discrepancies are unavoidable, and as a result, the particle can "drift" under the influence of the aligning magnets while in the absence of a driving magnetic field. In order to quantify the drift inherent in the apparatus, we performed tests to determine an upper bound for uncertainty in our experiments. This speed, $U \approx 1$ μm/s, serves a baseline for our results; speeds below this value should not be considered robust evidence of propulsion in this context.

The actuated particles are immersed in an aqueous solution of hexadecyltrimethylammonium bromide (CTAB; Sigma Aldrich, H5882) and sodium salicylate (NaSal; Sigma Aldrich, S2679) in deionized water and held in a glass container 50 mm in diameter and 30 mm tall, large enough to avoid wall effects.[27] CTAB, a common cationic surfactant, comprises a hydrophilic head and a hydrophobic tail.[49] These molecules self-assemble through a balance of weak polar repulsions and attractions into structures, known as micelles, at sufficient concentrations or when in the presence of salts or counter-ions.[34,49] NaSal is known to promote the growth of cylindrical (hence wormlike) micelles.[49] These micelles then entangle and form networks that break under sufficient stress and heal during relaxation.[34] Solutions are prepared by slowly adding 130 mM CTAB to a solution of 130 mM NaSal and allowed

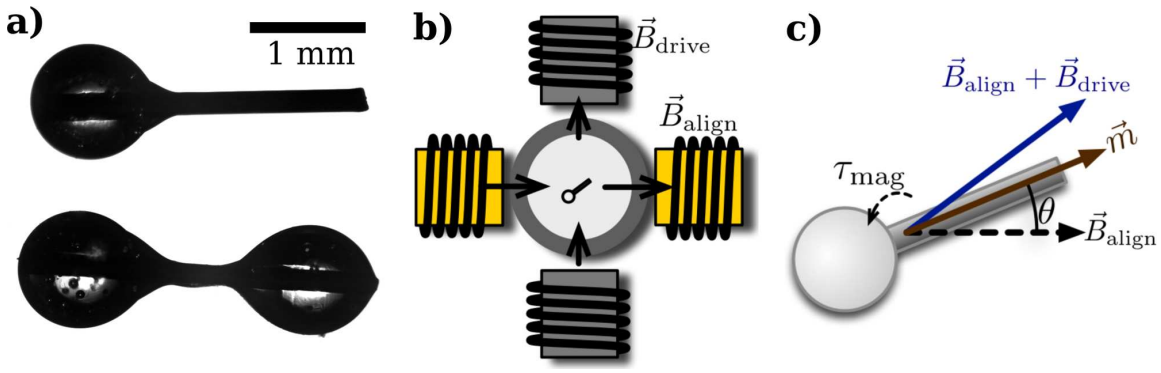

FIG. 1. **(a)** The two geometries investigated: (i) asymmetric and (ii) symmetric particle. **(b)** Apparatus consisting of one pair of aligning magnets orthogonal to a second pair of driving magnets. **(c)** Schematic of particle and apparatus.

to mix overnight. These are then degassed at room temperature using a vacuum chamber at -13 psi for several hours until any bubbles have been removed.

The rheological properties of the wormlike micellar (WLM) solution, shown in Fig. 2, are characterized by a cone-and-plate, stress-controlled rheometer (RFS3, TA Instruments). Figure 2(a) shows the steady behavior of viscosity μ and shear stress σ as a function of shear rate $\dot{\gamma}$. The observed plateau in shear stress between $0.5 \lesssim \dot{\gamma} \lesssim 10$ is a well-known feature of WLM solutions and is often referred to as the unstable or plateau region, in which the same shear stress can support multiple strain rates.[34,35] This indicates that increasing or decreasing the applied shear stress through this unstable region will likely result in shear banding.[34,35] This further implies that there can be local, abrupt variations in viscosity, as this solution exhibits strong shear thinning tendencies due to the aligning and breaking of WLM networks.[34] The shear-thinning viscosity behavior of the WLM solution can be characterized by fitting the rheological data to the Carreau-Yosuda model

$$\mu(\dot{\gamma}) = \mu_\infty + (\mu_0 - \mu_\infty)(1 + (\lambda_{Cr}\dot{\gamma})^2)^{\frac{n-1}{2}}, \tag{1}$$

where $\mu(\dot{\gamma})$ is the effective viscosity of the fluid as a function of shear rate $\dot{\gamma}$, μ_0 is the zero-shear viscosity, μ_∞ is the infinite-shear viscosity, and n is the power law index of the fluid.[50] The quantity λ_{Cr} is a characteristic timescale or inverse shear rate at which the fluid transition from Newtonian-like to power law behavior. This transition is often characterized by the Carreau number $Cr = \lambda_{Cr}\dot{\gamma}$. If $Cr < 1$, then the fluid viscosity behaves Newtonian-

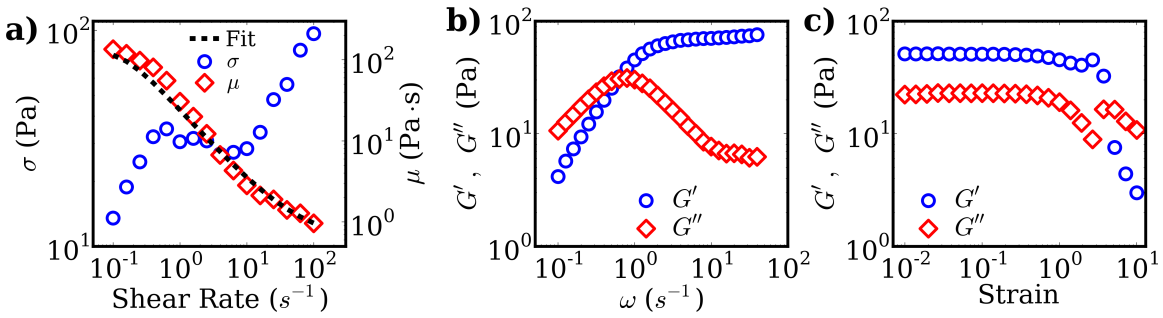

FIG. 2. **(a)** Shear viscosity μ and shear stress σ as a function of shear rate $\dot{\gamma}$. Shear-thinning viscosity is modeled as a Carreau fluid (dashed line). Note the stress plateau over $(0.5 \lesssim \dot{\gamma} \lesssim 10)$. This plateau, where increasing shear rate does not result in increasing stress, is characteristic of fluids which support shear banding. **(b)** Storage (G') and loss (G'') moduli as a function of angular frequency ω at strain amplitude of 0.01. The inverse of the frequency where G' and G'' cross ($\omega_c \approx 0.64$ s^{-1}) defines a characteristic timescale of the fluid ($\lambda \approx 1.56$ s). **(c)** G' and G'' as a function of strain at angular frequency $\omega = 2$ s^{-1}. Note that the WLM solution becomes highly nonlinear above a strain amplitude of 1.

like; if $Cr > 1$, then the fluid viscosity is shear thinning.[50] Using a least squares fit, we find that $\mu_0 \approx 137$ Pa·s, $\mu_\infty \approx 0.6$ Pa·s, $\lambda_{Cr} \approx 6.9$ s, and $n \approx 0.1$. With these value, we can estimate an upper bound for the Reynolds number $Re = \frac{\rho(\dot{\theta} R_{\text{dimer}})(2R_{\text{dimer}})}{\mu_\infty}$. Using the above values, we find that the upper bound for Re is approximately 0.3, which indicates that inertial effects may be neglected.

We can further characterize the WLM solution using oscillatory rheology. Figure 2(b) shows the elastic (storage) G' and viscous (loss) G'' moduli as a function of angular frequency ω at strain amplitude of 0.01. The fluid behavior is dominated by viscous dissipation (G'') at low frequencies and by elasticity (G') at higher frequencies. Figure. 2(c) suggests that above a strain of 1 (or 100%) at $\omega = 2$ s^{-1}, the rheology of the solution becomes highly nonlinear. These large amplitudes are most apt to cause "damage" to the micellar structures.

We define a characteristic timescale λ, which corresponds to the traditionally defined reptation time combined with the equilibrium timescale for the scission and reformation of micellar structures.[39,51,52] Measuring or estimating λ is not a trivial task. Here we estimate λ from oscillatory rheology by interpolating the angular frequency ω where $G' = G''$ and then taking the inverse (Fig. 2(b)).[52] One could also estimate λ using steady rheology by

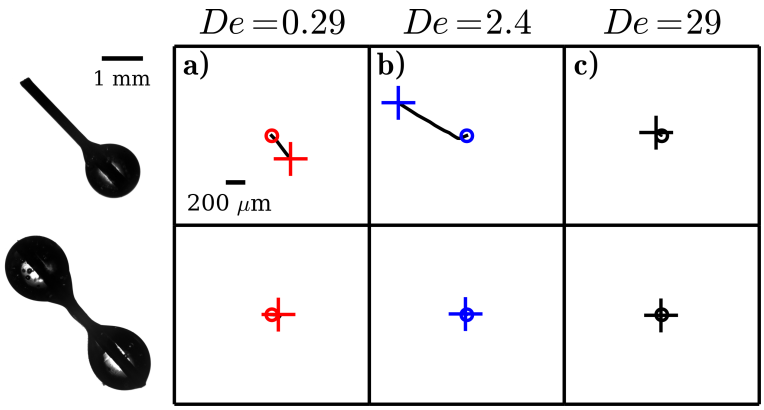

FIG. 3. Trajectories from ∘ to + for asymmetric and symmetric particles actuated at frequencies corresponding to three values of De for 60-80 s. The asymmetric particle exhibits robust propulsion at $De = 0.29$ and $De = 2.4$ towards the bead and rod respectively. No propulsion is observed for the symmetric particle or for the asymmetric particle at $De = 29$; these small displacements are within the drift velocity of the apparatus.

taking the inverse of the approximate shear rate at which shear stress enters the plateau region (Fig. 2(a)).[52] In our case, both methods yield $\lambda \approx 1.56$ s.

Now that we have estimated the value of λ, we can define two very important dimensionless parameters, namely the Deborah number De and the Weissenberg number Wi. Here, $De = \lambda\omega = 2\pi\lambda f$ and $Wi = \lambda|\dot{\gamma}|$. Note that, for Newtonian fluids, $De = Wi = 0$. In the context of our actuated particle in a WLM solution, low De ($De \ll 1$) suggests that the fluid has sufficient time to relax and reform its micellar network between particle reorientations, while high De ($De \gg 1$) indicates that damaged micelles are unable to reform. Most importantly, intermediate $De \sim 1$ indicates that the oscillation of the particle could potentially couple with the relaxation of the fluid, as each new oscillation occurs under the influence of the "fading memory" of the previous cycle, while not oscillating so quickly that the micellar structures are completely broken apart. In addition, the Wi can be viewed as the propensity of the particle's motion to deform the micellar structures, with high Wi flows more likely to stretch or break the micellar network and to produce fluid instabilities.[53]

III. EXPERIMENTAL RESULTS

For a Newtonian fluid at these low Reynolds ($Re < 0.3$), we would not expect a reciprocally actuated particle, regardless of geometry, to achieve any appreciable net motion. A very different behavior, however, is found when the same particle is placed in a wormlike micellar (WLM) solution that is shear-thinning, viscoelastic, and prone to shear band formation. Despite the lack of inertia, we find that the reciprocally actuated particle is able to translate through the WLM medium (Fig. 3).

Figure 3 shows the displacement of both the asymmetric and symmetric particles immersed in a WLM solution at three values of De. At $De = 0.29$, we observe the asymmetric particle moving parallel to the aligning field in the direction of the bead (Fig. 3(a)), and negligible translation for the symmetric particle. In the case of $De = 2.4$, we again observe propulsion parallel to the aligning field but in the direction of the rod (Fig. 3(b), and once again, the symmetric particle does not appreciably translate. Lastly, at $De = 29$, we find that neither the asymmetric nor the symmetric particle exhibits propulsion. We note that neither the symmetric nor the asymmetric particle shows any net translation or motion in Newtonian fluids under similar conditions. These observations indicate that the nonlinear rheology of the WLM solution is able to break the scallop theorem. Also, it seems that an asymmetric geometry is critical to breaking time-reversal symmetry in such solutions. In addition, we find three distinct regimes exhibited by the reciprocally actuated particle in a WLM solution: (i) low De or $De < 1.0$, where the asymmetric particle moves toward the bead; (ii) intermediate De or $De \sim 1$, where the particle moves toward the rod, and (iii) high De or $De > 10$, where the bead does not appreciably move.

We now quantify this fluid-induced propulsion shown in Fig. 3 by tracking the centroid of the particle over time. Figure 4 shows the tangential displacement of the asymmetric particle when actuated for 60-80 s. We find that at $De = 0.29$, the particle translates 200 μm in 4 cycles towards the bead (□). In contrast, for $De = 2.4$, the particle moves roughly 700 μm in 16 cycles (○), but this time in the direction of the rod. The third case, $De = 29$ (black line), exhibits a small displacement, only 80 μm over 320 cycles, and is roughly equal to the drift speed observed for these experiments, denoted by the shaded area. In what follows, we more closely examine these observations, discuss the transitions among the three observed regimes, and provide a potential mechanism to explain the behavior of this

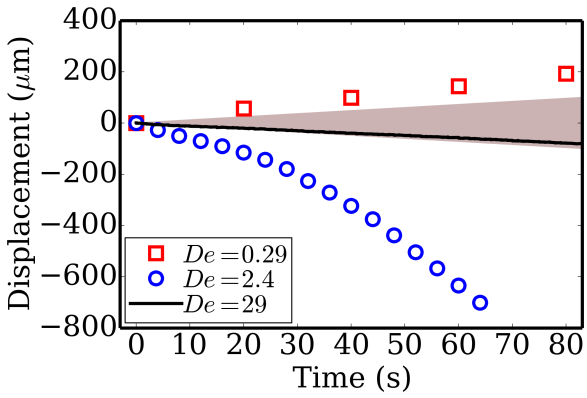

FIG. 4. Stroboscopic centroid displacement of the asymmetric particle tangent to the aligning field as a function of time at three different values of $De = 2\pi\lambda f$. The shaded region denotes the maximum drift velocity of the particle in the absence of a driving field.

reciprocal asymmetric particle in WLM solutions.

IV. DISCUSSION

After identifying the three regimes discussed above, we would like to further examine the transition of the particle from the regime with propulsion towards the bead ($De = 0.29$) to the regime with propulsion towards the rod ($De = 2.4$), as well as explain the lack of propulsion at $De = 29$. Figure 5(a) shows propulsion speed as a function of De and Fig. 5(b) shows the displacement per actuation cycle, which more clearly map the dependence of propulsion on De. A positive velocity and displacement per cycle indicate the particle moves tangential to the aligning field and towards the bead. A negative velocity represents motion in the opposite direction, towards the rod. At $De < 1.0$ (low De) we observe robust and repeatable propulsion, with large displacements per cycle ($\sim 75\ \mu m$) in the direction of the bead. Between $1.0 < De < 10$ ($De \sim 1$, intermediate De), the particle moves rapidly towards the rod, again with large displacements per cycle ($\sim 75\ \mu m$). There is a sharp peak at $De \approx 2.5$, and here the particle achieves speeds as high as $20\ \mu m/s$. Lastly, at $De > 10$ (high De), we observe very little propulsion, with speeds roughly equal to the maximum drift speed for our apparatus in the direction of the rod and negligible displacements per cycle.

What are the main mechanisms leading to this unexpected behavior? We believe the

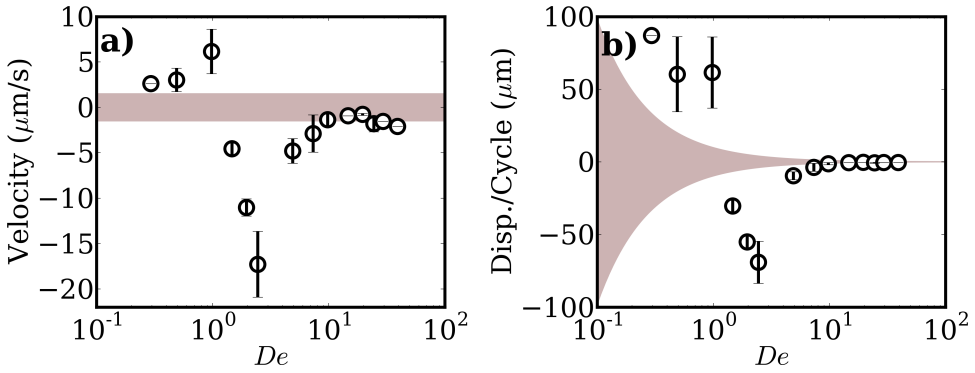

FIG. 5. **(a)** Velocity and **(b)** displacement per cycle as a function of De. A positive velocity and displacement per cycle indicate the particle moves tangential to the aligning field and towards the bead. A negative velocity represents motion in the opposite direction, towards the rod. Note the rapid transition from negative to positive velocities near $De = 1$. The shaded area represents the maximum drift velocity ($\sim 1\ \mu m/s$) and therefore provides an upper bound for uncertainty.

propulsion mechanism at low De is an imbalance in the first normal stress difference ($N1$), normal to curved streamlines, between the two ends of the particle. Shear forces along curved streamlines can deform polymers non-uniformly, ultimately producing a force in the radial direction.[53] The rod end of the particle has a greater curvature than the bead end, and as a result, the effects of this non-uniform deformation are more pronounced at the rod end of the particle. This imbalance produces a net force in the direction of the bead. Propulsion of this type has been previously observed for an asymmetric reciprocal dimer in dilute polymeric (viscoelastic) solution with relatively constant shear viscosity.[27] The velocity and displacement data shown in Figure 5 demonstrate a clear transition, occurring in the vicinity of $De = \lambda\omega = 1$, which causes the particle to reverse direction. This indicates that the transition occurs when the period of driving is roughly equal characteristic timescale λ of the WLM solution. For WLM solutions, the characteristic timescale λ not only represents a bulk relaxation time of the fluid, but also a timescale for the damaged micelles network to reform. At low De ($De < 1.0$), the micellar network has enough time to repair and heal all or nearly all damage caused by the last reorientation of the particle. However, at intermediate De, the actuated particle encounters parts of the network that have not fully relaxed and/or healed during rotation. At large De ($De > 10$), the lack of propulsion suggests that the micellar structures are ripped apart by the motion of the particle and are unable to reform or

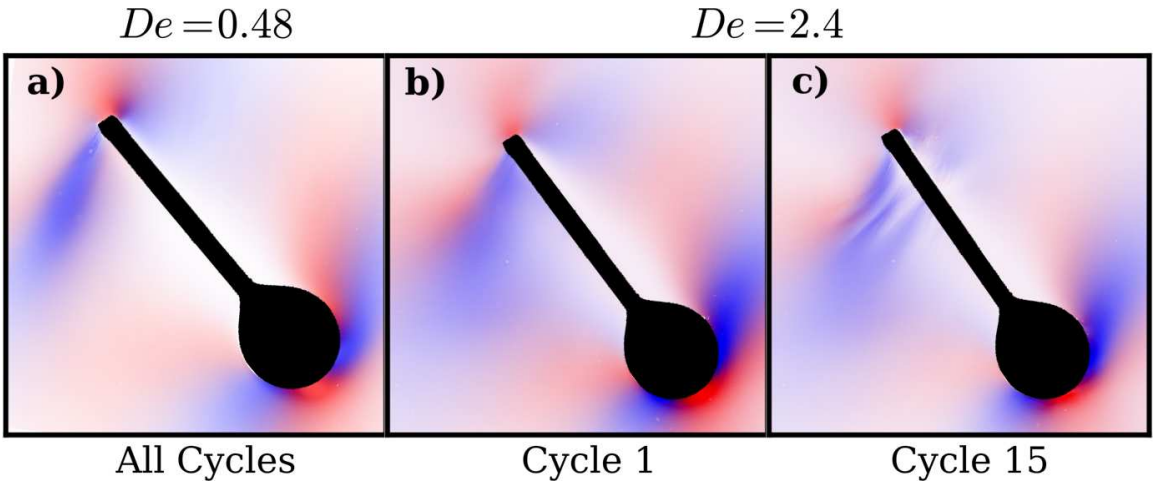

FIG. 6. (Color available online) Three snapshots of the particle oriented 3 degrees relative to the aligning field and rotating clockwise. Two complimentary polarization angles are shown in blue and red; blue indicates cross-polarizers parallel and orthogonal to the aligning magnetic field, while red shows light observed with cross-polarizers rotated 45 degrees relative to the blue axes. Intensity indicates the magnitude of birefringence detected **(a)** Detection of birefringence at $De = 0.48$; all cycles look identical. **(b)** Detection of birefringence at $De = 2.4$ after one cycle. Note the similarity with $De = 0.48$. **(c)** Detection of birefringence at $De = 2.4$ after 15 cycles. Note the development of recurring striations indicating structure at the rod-end of the particle.

heal. We can think of the micelles in this case as "fluidized," removing the non-linear effects of the micellar network that would induce propulsion. Given that we observe a transition near $De = 1$, and negligible propulsion above $De = 10$, we believe that whether the micellar network has time to reform is crucial to the propulsion mechanism of the particle, and that the rate of healing relative to the frequency of motion dictates the direction the particle will translate.

Since the velocity and displacement data in Fig. 5 show that the propulsion mechanism is likely connected to the microstructure, we examine the effects of the particle's motion using birefringence, a technique commonly used to study structure and fracture in WLM solutions.[36–39,54] High speed video is taken at 150 frames per second while placing the WLM solution and particle between two cross-polarizers. When the WLM solution is isotropic, all light is extinguished by the second polarizer. However, when the WLM solution possesses some anisotropy in its network structure, it becomes birefringent (with an index of refraction

depending on polarization direction) and can therefore effectively rotate the polarization of transmitted light. This rotated light is then partly admitted by the second polarizer and detected by the camera. In order to better capture the orientation of the network, we have created a composite with two complementary polarization angles shown in blue and red. Blue indicates cross-polarizers parallel and orthogonal to the aligning magnetic field, while red shows light observed with cross-polarizers rotated 45 degrees relative to the blue axes (Fig. 6(a)).

Figure 6 shows these composite images of birefringence for $De = 0.48$ (low De) and $De = 2.4$ (intermediate De) during the motion of the particle. Two images are shown at $De = 2.4$, with Fig. 6(b) and Fig. 6(c) corresponding to the first and fifteenth cycles respectively. In all three panels, birefringence is detected near the rod and the bead. These areas indicate stress-induced anisotropy in the micellar network in those regions. The patterns detected at $De = 0.48$ (Fig. 6(a)) and the first cycle at $De = 2.4$ (Fig. 6(b)) look qualitatively similar. However, of particular interest are the striations (alternating patches of white and blue) formed along the rod in Fig. 6(c). The development of these structures coincides with an increase in $\overline{Wi} = \lambda|\overline{\dot{\gamma}}|$, where $|\overline{\dot{\gamma}}|$ is the average shear rate per cycle, from $\mathcal{O}(1)$ at low De to $\mathcal{O}(10)$ at intermediate De. It has been shown that fluid instabilities become more likely in polymeric and WLM solutions with increasing strain rate or Wi;[36,53] Wi is often considered a measure of the non-linearity and stability of the fluid network. The striations in Figure 6(c) suggest that there may be a fluid instability present near the rod, and that the particle is locally fracturing the micellar network and remodeling it into structures aligned with its rotation.[36,38,39]

The observation that structures develop with repeated shearing of the micellar networks should be reflected in the displacement data of the particle in Fig. 4. In fact, we observe that the displacement per cycle is constant at $De = 0.29$, but at $De = 2.4$, there is a transient. This transient behavior is paralleled by the development of striations in the birefringence images over many cycles (Fig. 6(b,c)). This requires both high Wi to generate the spatial instability evident in the striations and $De > 1.0$ so that the micellar network cannot relax between reorientations, making the instability cumulative and the network anisotropy persistent. This persistence is evident in Figure 7, which shows the anisotropy of the micellar network in the frame immediately before the square wave switches sign to initiate a new half-cycle of motion. Figure 7(a) shows isotropy (absence of birefringence) in

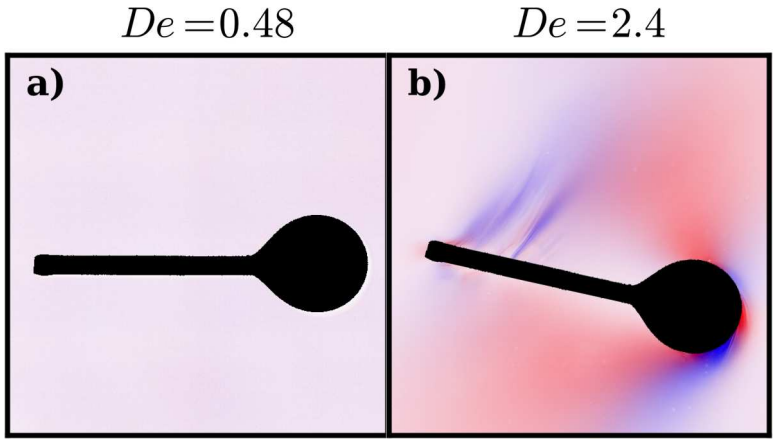

FIG. 7. (Color available online) **(a)** Absence of birefringence detected before the reversal in sign of the driving square wave at $De = 0.48$. The fluid's network structure has relaxed to an isotropic equilibrium state. **(b)** Birefringence detected before the reversal in sign of the driving square wave at $De = 2.4$. Note that the structures formed during the rotation of the particle at intermediate De persist for the entirety of each cycle.

the network around the rod at $De = 0.48$. In stark contrast, Fig. 7(b) clearly shows that at $De = 2.4$, anisotropies in the network developed during the rotation of the particle are still present before the beginning of a new half-cycle of motion. In other words, the remodeling of the network that occurred during rotation (due to increased $\overline{Wi}$) has been "locked in" due to $De \gtrsim 1$. The combination of the anisotropy and the inability for the network to relax likely has significant consequences for the normal stress differences discussed in the proposed mechanism for low De. First, the structure formed at the rod indicates that the micellar network is likely already aligned and most likely still stretched, suggesting that the micelles in this area cannot produce a normal stress response corresponding to the instantaneous streamline curvature. Second, the particle on a whole is operating at higher average strain rate, so any normal stress differences produced at the bead should be relatively larger in magnitude.[53] These two effects, a strong reduction in normal stress difference at the rod and an enhancement in normal stress difference at the bead, could lead to a not only to a reversal in the direction of the imbalance in normal stress difference, but also to an imbalance of greater magnitude, consistent with the increased speed at $De \sim 1$ relative to $De < 1.0$ (see Fig. 5(a)).

V. CONCLUSION

In this paper, we have demonstrated that net motion or propulsion is possible for reciprocally actuated, rigid particles immersed in a wormlike micellar (WLM) solution even at low Reynolds number; no propulsion is observed with Newtonian fluids under similar conditions (not shown). We investigated this fluid-induced propulsion in WLM solutions using tracking methods as well as birefringence, which is used to obtain information on the fluid microstructure. We find different propulsion regimes depending on the Deborah number ($De = \lambda\omega = 2\pi\lambda f$): net motion towards the bead at low De, net motion towards the rod at intermediate De, and no propulsion at high De. At low De, we believe propulsion is caused by an imbalance in the first normal stress differences between the two ends of the particle (bead and rod); the higher relative curvature of the streamlines near the rod when compared to those near the bead generates a net force in the direction of the bead. In this regime, the WLM solution has ample time to relax each time it is sheared, and therefore the response of the fluid to the particle is one characteristic of other viscoelastic fluids.[27] However, at $De \sim 1$, we observe network anisotropy near the rod using birefringence, possibly caused by a fluid instability, which indicates alignment of the micellar structure. This alignment is "locked in," due to the shorter timescale of the particle relative to the fluid. Therefore, the particle is actively altering the local properties of the fluid at the rod, and this network remodeling reduces the normal stress differences produced there. Coupled with enhanced normal stress differences at the bead due to an increased average shear rate, the imbalance increases in magnitude and reverses direction, propelling the particle in the direction of the rod at speeds an order of magnitude greater than observed in dilute polymeric solutions.

This work adds to our understanding of swimming in complex media, in particular in fluids with networks. Here, the interplay between structural relaxations of WLM solutions and reciprocal actuation results in two directions of propulsion, primarily distinguished by the timescale of the stroke. This shows that the general principle of propulsion enabled by nonlinear rheology can in fact take many forms, depending on fluid microstructure, swimmer geometry, and stroke. By extension, these experiments also suggest a broad range of possibilities for artificial micro-swimmers in complex media for use in targeted drug delivery, lab-on-a-chip devices, and collective self-assembly.

ACKNOWLEDGMENTS

We thank Gabriel Juarez for helpful discussions. This work is supported by the Army Research Office through award W911NF-11-1-0488. DAG was supported by an NSF Graduate Research Fellowship.

REFERENCES

[1]C. Brennen and H. Winet, "Fluid mechanics of propulsion by cilia and flagella," Annu. Rev. Fluid Mech. **9**, 339–398 (1977).

[2]J. Gray, "The movement of sea-urchin spermatozoa," J. Exp. Biol. **32**, 775–801 (1955).

[3]J. Gray and G.J. Hancock, "The propulsion of sea-urchin spermatozoa," J. Exp. Biol. **32**, 802–814 (1955).

[4]N. Cohen and J.H. Boyle, "Swimming at low reynolds number: a beginners guide to undulatory locomotion," Comtemporary Physics **51**, 103–123 (2010).

[5]J. Gray and H.W. Lissmann, "The locomotion of nematodes," J. Exp. Biol. **41**, 135–154 (1964).

[6]E. Lauga and T. Powers, "The hydrodynamics of swimming microorganisms," Reports on Progress in Physics **72**, 096601 (Sep. 2009).

[7]J. Lighthill, "Flagellar hydrodynamics," SIAM Rev. **18**, 161–230 (1976).

[8]E.M. Purcell, "Life at low reynolds number," Am. J. Phys. **45**, 3–11 (197).

[9]H.C. Berg and L. Turner, "Torque generated by the flagellar motor of escherichia coli," Biophys. J. **65**, 2201–2216 (1993).

[10]J. Korta, D.A Clark, C.V. Gabel, L. Mahadevan, and A. Samuel, "Mechanosensation and mechanical load modulate the locomotory gait of swimming c. elegans," J. Exp. Biol. **210**, 2383–2389 (2007).

[11]D.F. Katz, R.N. Mills, and T.R. Pritchett, "The movement of human spermatozoa in cervival mucus," J. Reprod. Fertil. **53**, 259–265 (1978).

[12]G.V. Eriksen, I. Carlstedt, N. Uldbjerg, and E. Ernst, "Cervical mucins affect the motility of human spermatozoa in vitro," Fertil. Steril. **70**, 350–354 (1998).

[13]C. Montecucco and R. Rappuoli, "Living dangerously: How helicobacter pylori survives in the human stomach," Nat. Rev. Mol. Cell Bio. **2**, 457–466 (2001).

[14]J.P. Celli, B.S. Turner, N.H. Afdhal, S. Keates, I. Ghiran, C.P. Kelly, R.H. Ewoldt, G.H. McKinley, P. So, S. Erramilli, and R. Bansil, "Heliobacter pylori moves through mucus by reducing mucin viscoelasticity," Proc. Natl. Acad. Sci. USA **106**, 14321–14326 (2009).

[15]L. Zhu, E. Lauga, and L. Brandt, "Self-propulsion in viscoelastic fluids: Pushers vs. pullers," Phys. Fluids **24**, 051902 (2012).

[16]H.C. Fu, T.R. Powers, and C.W. Wolgemuth, "Theory of swimming filaments in viscoelastic media," Phys. Rev. Lett. **99**, 258101 (2007).

[17]J. Teran, L. Fauci, and M. Shelley, "Peristaltic pumping and irreversibility of a Stokesian viscoelastic fluid," Phys. Fluids **20**, 073101 (Jul 2008).

[18]J. Teran, L. Fauci, and M. Shelley, "Viscoelastic fluid response can increase the speed and efficiency of a free swimmer," Phys. Rev. Lett. **104**, 4.

[19]S.E. Spagnolie, B. Liu, and T.R. Powers, "Locomotion of helical bodies in viscoelastic fluids: Enhanced swimming at large helical amplitudes," Phys. Rev. Lett. **111**, 068101 (2013).

[20]B. Liu, T.R. Powers, and K.S. Breuer, "Force-free swimming of a model helical flagellum in viscoelastic fluids," PNAS **108**, 19516–19520 (2011).

[21]X.N. Shen and P.E. Arratia, "Undulatory swimming in viscoelastic fluids," Phys. Rev. Lett. **106**, 208101 (May 2011).

[22]J. Espinosa-Garcia, E. Lauga, and R. Zenit, "Fluid elasticity increases the locomotion of flexible swimmers," Phys. Fluids **25**, 031701 (2013).

[23]T. Normand and E. Lauga, "Flapping motion and force generation in a viscoelastic fluid," Phys. Rev. E **78**, 061907 (Dec 2008).

[24]O.S. Pak, T. Normand, and E. Lauga, "Pumping by flapping in a viscoelastic fluid," Phys. Rev. E **81**, 036312 (Mar 2010).

[25]E. Lauga, "Life at high Deborah number," Europhys. Lett. **86**, 64001 (Jul 2009).

[26]H.C. Fu, C.W. Wolgemuth, and T.R. Powers, "Swimming speeds of filaments in nonlinearly viscoelastic fluids," Phys. Fluids **21**, 033102 (Mar 2009).

[27]N.C. Keim, M. Garcia, and P.E. Arratia, "Fluid elasticity can enable propulsion at low reynolds number," Phys. Fluids **24**, 081703 (2012).

[28]G. Juarez, K. Lu, J. Sznitman, and P. E. Arratia, "Motility of small nematodes in wet granular media," EPL **92**, 44002 (2010).

[29]S. Jung, "Caenorhabditis elegans swimming in a saturated particulate system," Phys.

Fluids **22**, 6 (Mar 2010).

[30]L.J. Fauci and R. Dillon, "Biofluidmechanics of reproduction," Annu. Rev. Fluid Mech. **38**, 371–394 (2006).

[31]M.W. Harman, S.M. Dunham-Ems, M.J. Caimano, A.A. Belperron, L.K. Bockenstedt, H.C. Fu, J.D. Radolf, and C.W. Wolgemuth, "The heterogenous motility of the lyme disease spirochete in gelatin mimics dissemination through tissue," Proc. Natl. Acad. Sci. USA **109**, 3059–3064 (2012).

[32]C. Josenhans and S. Suerbaum, "The role of motility as a virulence factor in bacteria," Int. J. Med. Microbiol. **291**, 605–614 (2002).

[33]M. Alexander, *Introduction to soil microbiology* (R.E. Krieger, Malabar, FL, 1991).

[34]E. Miller and J.P. Rothstein, "Transient evolution of shear-banding wormlike micellar solutions," J. Non-Newtonian Fluid Mech. **143**, 22–37 (2007).

[35]P.C.F. Mller, S. Rodts, M.A.J. Michels, and D. Bonn, "Shear banding and yield stress in soft glassy materials," Phys. Rev. E **77**, 041507 (2008).

[36]M.-A. Fardin and S. Lerouge, "Instabilities in wormlike micelle systems," Eur. Phys. J. E. **35**, 91 (2012).

[37]J.P. Rothstein, "Strong flows of viscoelastic wormlike micelle solutions," Ann. Rheol. Reviews, 1–45(2009).

[38]B. Akers and A. Belmonte, "Impact dynamics of a solid sphere falling into a viscoelastic micellar fluid," J. Non-Newtonian Fluid Mech. **135**, 97–108 (2006).

[39]J.R. Gladden and A. Belmonte, "Motion of a viscoelastic micellar fluid around a cylinder: Flow and fracture," Phys. Rev. Lett. **98**, 224501 (2007).

[40]A.M. Leshansky, "Enhanced low-reynolds-number propulsion in heterogeneous viscous environments," Phys. Rev. E **80** (2009).

[41]H.C. Fu, V.B. Shenoy, and T.R. Powers, "Low-reynolds-number swimming in gels," EPL **91** (2010).

[42]D.A. Gagnon, X.N. Shen, and P.E. Arratia, "Undulatory swimming in fluids with polymer networks," Europhys. Lett.(2013).

[43]H.C. Berg and L. Turner, "Movement of microorganisms in viscous environments," Nature **278**, 349–351 (1979).

[44]M.E. Cates and S.J. Candau, "Statics and dynamics of worm-like surfactant micelles," J. Phys.: Condens. Matter **2**, 6869–6892 (1990).

[45]G. Ianniruberto and G. Marrucci, "Convective orientational renewal in entangled polymers," J. Non-Newtonian Fluid Mech. **95**, 363–374 (2000).

[46]S.T. Milner, T.C.B. McLeish, and A.E. Likhtman, "Microscopic theory of convective constraint release," J. Rheol. **45** (2000).

[47]R.S. Graham, A.E. Likhtman, T.C.B McLeish, and S.T. Milner, "Microscopic theory of linear, entangled polymer chains under rapid deformation including chain stretch and convective constraint release," J. Rheol. **47**, 1171–1200 (2003).

[48]J.M. Adams, S.M. Fielding, and P.D. Olmstead, "Transient shear banding in entangled polymers: A study using the rolie-poly model," J. Rheol. **55**, 1007–1032 (2011).

[49]C.A. Dreiss, "Wormlike micelles: where do we stand? recent developments, linear rheology and scattering techniques," Soft Matter **3**, 956–970 (2007).

[50]R.B. Bird, C.F. Curtiss, R.C. Armstrong, and O. Hassager, *Dynamics of Polymeric Liquids, Vol. 1* (Wiley, New York, 1987).

[51]L.M. Walker, "Rheology and structure of worm-like micelles," Curr. Opin. Colloid Interface Sci. **6**, 451–456 (2001).

[52]S. Rogers, J. Kohlbrecher, and M.P. Lettinga, "The molecular origin of stress generation in worm-like micelles, using a rheo-sans laos approach," Soft Matter **8**, 7831 (2012).

[53]P. Pakdel and G.H. McKinley, "Elastic instability and curved streamlines," Phys. Rev. Lett. **77**, 2459–2462 (1996).

[54]S.J. Haward and G.H. McKinley, "Stagnation point flow of wormlike micellar solutions in a microfluidic cross-slot device: effects of surfactant concentration and ionic environment," Phys. Rev. E Stat. Nonlin. Soft Matter Phys. **85**, 031502 (2012).